Probing the deuteron breakup and linking the cross sections of residue production between the neutron- and deuteron-induced spallation at 500 MeV/nucleon

Suyang Xu (徐苏扬), Guanming Yang (杨冠铭), Mengting Jin (金梦婷), and Jun Su (苏军)[*]

Sino-French Institute of Nuclear Engineering and Technology, Sun Yat-sen University, Zhuhai 519082, China

Background: Cross section data of neutron-induced spallation are requisite in order to study the transmutation of the long-lived fission products from the spallation. However, those data are very scarce at present due to the difficulty of providing a neutron source in the GeV region and the impossibility of the inverse dynamics.

Purpose: The present work is an attempt to probe the dynamic process of deuteron breakup in deuteron-induced spallation and discuss the possibility of measuring indirectly the cross section in neutron-induced spallation.

Method: The isospin-dependent quantum molecular dynamics model is applied to simulate the spallation process until the excitation energy of the hot fragment is less than 2 MeV/nucleon. The statistical model GEMINI based on the Hauser-Feshbach formalism is used to describe the deexcitation of the hot fragments.

Results: By comparing the calculations to the data, the theoretical framework is proved to be reasonable when predicting the neutron production in spallation. By investigating the deuteron breakup, deuteron-induced spallation is divided into deuteron absorbing, neutron stripping, proton stripping, and elastic breakup. It is found that the proton stripping plays the dominant role in the production of high-energy neutrons, while the neutron stripping is responsible for the emission of high-energy protons. Due to the weak binding of the deuteron, it is suggested that the combination of neutron stripping and elastic breakup in deuteron-induced spallation is equivalent to neutron-induced spallation.

Conclusions: Using the proton recoiling from the deuteron as the trigger signal, deuteron-induced spallation may be applied to measure indirectly the cross section in neutron-induced spallation.

I. INTRODUCTION

In the early 1990s, when the climate change issue appeared in public view, nuclear power plants began to play a role in the electric power system, as they do not release large amounts of pollutants into the atmosphere in the process of power generation [1]. As demand for nuclear power grows, uranium consumption will increase and a large amount of radioactive waste will be produced at the same time [2–4]. High-level radioactive waste, which is the most harmful component of spent nuclear fuel, can be disposed of in two possible ways: emplacement far away from human activity and transmutation into short-lived or stable nuclei [5]. The first way will continuously aggravate the geological burden in the long term [6]. On the other hand, people have paid much attention to the research field of the nuclear transmutation since the concept was put forward [7–10].

According to its charge number, high-level radioactive waste is divided into two main components: the minor actinides and the long-lived fission products (LLFPs) [11]. Because the transmutation of the minor actinide lies principally in the fast neutron capture mechanism, fast reactors and accelerator driven subcritical systems (ADSs) are being constructed for investigation of transmutation [12]. However,

little attention has been paid to the LLFPs for two reasons. First, there is no heat released in the transmutation process of the LLFPs. If the LLFPs are put in an ADS, the output power of the reactor will decrease. Second, the neutron capture cross section of the LLFPs is small. They cannot be transmuted by neutron capture like minor actinides. Nevertheless, the continuous production of LLFPs is inevitable in the operation of conventional nuclear power plants and ADSs, which will be put into operation in the coming years. As a result, reliable and effective methods need to be found in order to reduce their amount.

Spallation, as the basis mechanism to produce high-energy neutrons in ADSs, is proposed to be suitable for the transmutation of LLFPs [13]. Recently, several experimental studies on the spallation reactions of LLFPs showed that the proton- and deuteron-induced spallation are promising mechanisms for the transmutation of LLFPs [14]. Compared to charged particle beams (proton and deuteron), the neutron has a larger range in matter and hence can cause more spallations before it is moderated. Therefore, data on neutron-induced spallation are requisite in order to study the transmutation of the LLFPs by spallation [15]. On the other hand, according to the existing design scheme of ADSs, data on neutron-induced spallation are also needed to calculate the energy release rate in the coupler between the spallation neutron target system and the subcritical reactor [16–18]. However, those data are very scarce at present due to the difficulty of providing a neutron

---

*Corresponding author: sujun3@mail.sysu.edu.cn

source in the GeV region and the impossibility of the inverse dynamics [19–21].

Models have been applied to predict the neutron cross sections in spallation. In 2010, the International Atomic Energy Agency (IAEA) made efforts to upgrade a benchmark of spallation models which presented the results of the most widely used spallation codes [22]. In the IAEA benchmark, the codes describe in sequence the two mechanisms of spallation reactions: the intranuclear cascade (INC) and the deexcitation, which compose a two-step model of nuclear spallation. In our previous work, the two-step model was developed to describe the production of the intermediate-mass fragments (IMFs) dynamically [23]. The framework the of isospin-dependent quantum molecular dynamics (IQMD) model was applied, followed by use of the GEMINI code. The version of the IQMD model is IQMD-BNU, which was introduced and compared with the other versions in a transport-code comparison project [24,25]. In the present work, attention is paid to the deuteron-induced spallation of the LLFP ^{137}Cs.

The paper is organized as follows. In Sec. II, we describe the method. In Sec. III, we present both the results and discussions. Finally, summaries are given in Sec. IV.

II. THEORETICAL FRAMEWORK

A. Isospin-dependent quantum molecular dynamics model

In the IQMD model [26,27], the N-body system can be expressed by an N-body wave function, which is supposed to be the direct product of single-nucleon wave functions in coherent states. Through the application of a Gaussian wave packet, the N-nucleon wave function is given by

$$\phi(\mathbf{r}, t) = \prod_{i=1}^{N} \frac{1}{(2\pi L)^{3/4}} e^{-\frac{[\mathbf{r}-\mathbf{r}_i(t)]^2}{4L}} e^{\frac{i\mathbf{r}\cdot\mathbf{p}_i(t)}{\hbar}}, \quad (1)$$

where $\mathbf{r}_i$ and $\mathbf{p}_i$ represent respectively the average position and the mean momentum of the ith nucleon, and the parameter L is related to the square of the width of the Gaussian wave packet for each nucleon. In this paper, L is 1 fm^2.

By applying the Wigner transform, the phase-space density function of the system is described as follows:

$$f(\mathbf{r}, \mathbf{p}, t) = \sum_{i=1}^{N} \frac{1}{(\pi\hbar)^3} e^{-\frac{[\mathbf{r}-\mathbf{r}_i(t)]^2}{2L}} e^{-\frac{[\mathbf{p}-\mathbf{p}_i(t)]^2 2L}{\hbar^2}}. \quad (2)$$

Then the expression of local density is

$$\rho(\mathbf{r}, t) = \frac{1}{(2\pi L)^{3/2}} \sum_{i=1}^{N} e^{-\frac{[\mathbf{r}-\mathbf{r}_i(t)]^2}{2L}}, \quad (3)$$

which is obviously related to $\mathbf{r}$, the position of nucleon. In this system, the Hamiltonian is composed of the kinetic energy T, the Coulomb potential energy U_{Coul}, and the nuclear potential energy part:

$$H = T + U_{\text{Coul}} + \int V[\rho(\mathbf{r})]d\mathbf{r}. \quad (4)$$

In the third term, the nuclear potential energy density of the asymmetric nuclear matter with density ρ and asymmetry δ is

written as

$$V(\rho, \delta) = \frac{\alpha}{2}\frac{\rho^2}{\rho_0} + \frac{\beta}{\gamma+1}\frac{\rho^{\gamma+1}}{\rho_0^{\gamma}} + \frac{C_{sp}}{2}\left(\frac{\rho}{\rho_0}\right)^{\gamma_i}\rho\delta^2, \quad (5)$$

where ρ_0 is the normal density. The parameters used in this paper are $\alpha = -356.00$ MeV, $\beta = 303.00$ MeV, $\gamma = 7/6$, $C_{sp} = 38.06$ MeV, and $\gamma_i = 0.75$, and they give a compressibility of 200 MeV at saturation density for isospin symmetric nuclear matter.

In the framework of the generated mean-field theory, the time evolution of the nuclei in the system is determined by Hamiltonian equations of motion,

$$\dot{\mathbf{r}}_i = \nabla_{\mathbf{p}_i}H, \quad \dot{\mathbf{p}}_i = -\nabla_{\mathbf{r}_i}H. \quad (6)$$

Besides, the nucleon-nucleon (NN) collisions are included in the IQMD code to simulate the short-range repulsive residual interaction and to describe the random change of the phase space distribution. The differential cross sections of the NN collisions are assumed to be the direct product of the cross section of the NN collisions in free space, σ^{free}, the factor of the angular distribution, f^{angl}, and the in-medium correction factor, f^{med}:

$$\left(\frac{d\sigma}{d\Omega}\right)_i = \sigma_i^{\text{free}} f_i^{\text{angl}} f_i^{\text{med}}. \quad (7)$$

The subscript i is related to different channels of the nucleon-nucleon (NN) collisions, i.e., elastic proton-proton scatterings ($i = pp$), elastic neutron-proton scatterings ($i = np$), elastic neutron-neutron scatterings ($i = nn$), and inelastic nucleon-nucleon collisions ($i = \text{in}$). The parametrization of σ^{free} and f^{angl} is that of Ref. [28], and the in-medium factor f^{med} is taken from Ref. [29]. The in-medium factor for elastic scatterings is written as

$$f_{el}^{\text{med}} = \left(\sigma_0/\sigma_i^{\text{free}}\right)\tanh\left(\sigma_i^{\text{free}}/\sigma_0\right), \quad (8)$$

where $\sigma_0 = 0.85\rho^{-\frac{2}{3}}$. Because of the dependence of σ^{free} on the energy and isospin, f^{med} is dependent on the energy and isospin. For inelastic NN collisions, the NN-ND and ND-NN channels are included, where N denotes the nucleon and D denotes the delta particle. The cross sections and the decay width of delta particle are the same as in Ref. [30].

The initial configurations of nuclei are constructed in such a way that they yield the experimental binding energies and the central density 0.16 fm^{-3}. The coordinates are selected randomly in a sphere with $1.12 \times A^{1/3}$ as the radius and then scaled to yield the central density 0.16 fm^{-3}. The momenta are selected randomly in a Fermi sphere, then scaled to yield the experimental binding energy, in which the potential energy is calculated within the initial coordinates. For the deuteron, the initialization is different. The distance between the proton and neutron in the deuteron can be calculated with the experimental charge radius 2.14 fm. The potential energy and then the relative momentum can be calculated with the given distance and binding energy. The angles, both in the space and momentum, are selected randomly.

Otherwise, in order to enhance the stability of the N-body system, the Pauli blocking and the method of the phase space density constraint are taken into consideration. Through the

integration over a hypercube of volume h^3 in the phase space revolving around the point (r_i, p_i) at each time step, the space occupation probability $\bar{f}_i$ of the ith nucleon is given by

$$\bar{f}_i = \sum_n \delta_{\tau_n, \tau_i} \delta_{s_n, s_i} \int_{h^3} \frac{1}{\pi^3 \hbar^3} e^{-\frac{(\mathbf{r} - \mathbf{r}_n)^2}{2L} - \frac{(\mathbf{p} - \mathbf{p}_n)^2 L}{\hbar^2}} d^3r \, d^3p, \quad (9)$$

where τ_i and s_i represent respectively the isospin degree of freedom and the spin projection quantum number. At each time step, the phase space occupation probability is judged by an adjustable value k in the IQMD model. For each time $f_i > k$, the many-body elastic scattering will be applied to change the momentum of the ith nucleon. The scattering result is accepted only when all the phase space occupancies f_i at final states satisfy the condition $f_i < k$. In this paper, k is chosen to be 1.15.

B. GEMINI

The two-step model of nuclear spallation in the IAEA benchmark consists of two parts: the dynamical code and the statistical one. The dynamical part describes the excitation stage of the target nucleus impacted by the beams of incident particles, while the statistical part simulates the the emission of heavy fragments and light particles. On the basis of the model mentioned above, our present work includes additionally the decay process of the excited nucleus. A parameter E_{stop} is set in the IQMD model to restrict the maximal excitation energy of hot fragments formed in the excitation process. In this work, $E_{\text{stop}} = 2$ MeV/nucleon.

After hot fragments are formed by the execution of the IQMD model, the GEMINI code [31] is executed to obtain the cold ones. The Hauser-Feshbach formalism, which takes the spin degrees of freedom into consideration, is used to simulate the evaporation of light particles such as n, p, d, t, ^{3}He, α, ^{6}He, $^{6-8}$Li, and $^{7-10}$Be [32]. The partial decay width of excitation energy E^* and spin J_{CN} for the evaporation of the ith nucleon is

$$\Gamma_i(E^*, J_{\text{CN}}) = \frac{1}{2\pi \rho_{\text{CN}}(E^*, J_{\text{CN}})} \int \sum_{J_d=0}^{\infty} \sum_{J=|J_{\text{CN}}-J_d|}^{J_{\text{CN}}+J_d} \sum_{l=|J-S_i|}^{J+S_i} T_l(\varepsilon)$$
$$\times \rho_d(E^* - B_i - \varepsilon, J_d) d\varepsilon, \quad (10)$$

where J_d is the spin of the daughter nucleus. l, S_i, and J represent respectively the orbital, total, and spin angular momenta of the evaporated nucleus. ε and B_i are its kinetic and separation energies. T_l is its transmission coefficient and ρ refers to the level density. Transmission coefficients are calculated from the inverse reaction, which applies optical-model parameters obtained from global optical-model fits to elastic-scattering data.

III. RESULTS AND DISCUSSIONS

A. Neutrons produced in deuteron-induced spallation

In order to test the model, the double differential cross sections of neutrons produced in the spallation are calculated and compared to the available data. As examples, Fig. 1 presents the cases for $p + {}^{56}$Fe and $p + {}^{115}$In spallation reactions at
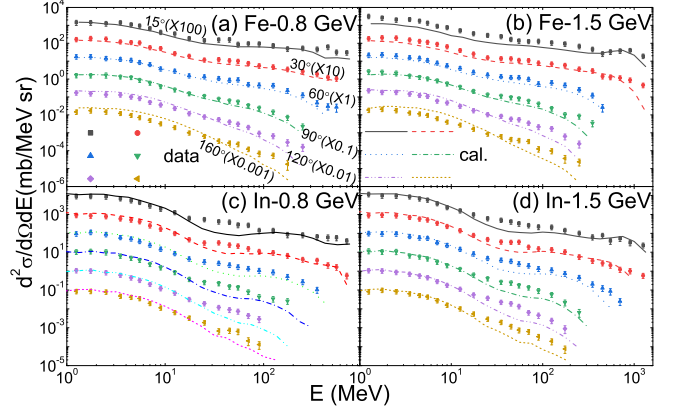

FIG. 1. Double differential cross sections of neutrons produced in $p + {}^{56}$Fe and $p + {}^{115}$In reactions at 800 and 1500 MeV/nucleon. The cross sections are scaled with factors 100, 10, 1, 0.1, 0.01, and 0.001, from $15°$ to $150°$. The calculations, shown as curves, are obtained by the IQMD + GEMINI model. The data, shown as points of different shapes, are taken from Ref. [33].

800 and 1500 MeV/nucleon. In general, the calculations agree with the data. The differences can be observed for the forward neutron at energies from 10 to 100 MeV/nucleon, especially for the $p + {}^{115}$In system. Since neutrons with energy larger than 100 MeV/nucleon will be the focus when studying the deuteron breakup in the following, we do not delve into the reason for the differences in the present work.

The calculations by the IQMD + GEMINI model are also compared to the predictions by the benchmark codes [34]. Examples are shown in Fig. 2 for the case of neutrons emitted at $60°$ from $p + {}^{56}$Fe spallation at 800 MeV/nucleon. Among these curves, the (red) thick one is the case calculated by the IQMD + GEMINI model. The comparison also shows the
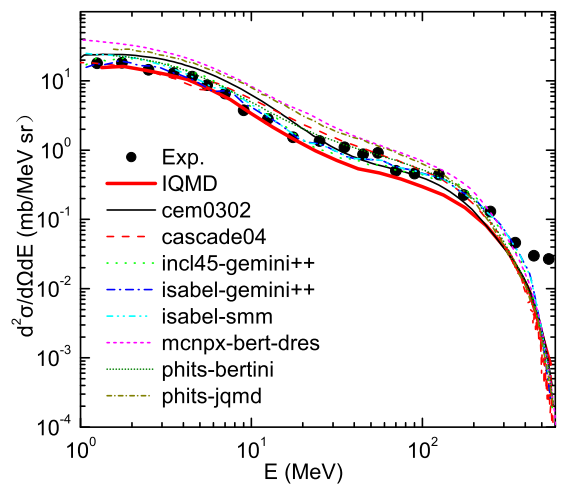

FIG. 2. Comparison of the neutron double differential cross sections at $60°$ predicted by the IQMD + GENINI model and some other models for $p + {}^{56}$Fe spallation at 800 MeV/nucleon. The calculations by the IQMD + GEMINI model are shown as a (red) thick curve. The predictions by other models are taken from Ref. [34]. Data taken from Ref. [33] are also shown.
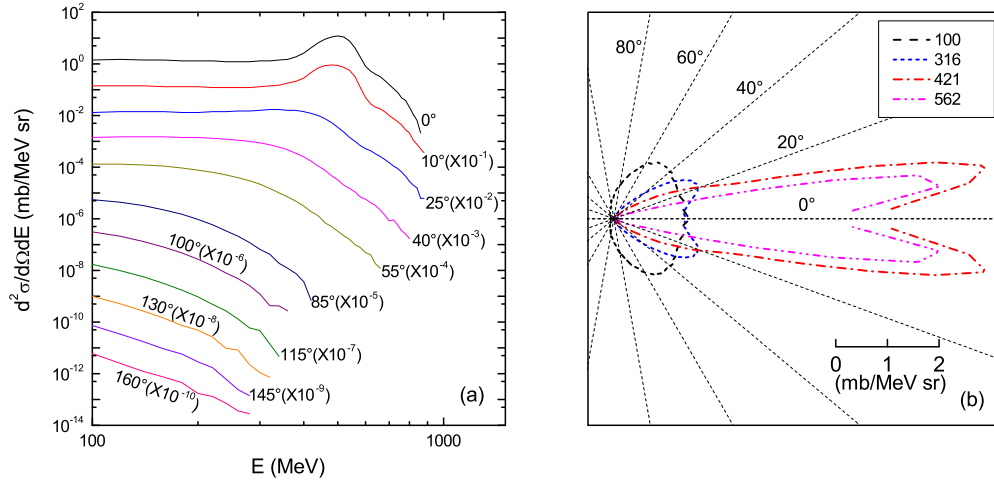
FIG. 3. Double differential cross sections of high-energy neutrons produced in $d + {}^{137}$Cs spallation at 500 MeV/nucleon. (a) The cross sections are scaled with factors from 1 to 10^{-10} respectively, for cases from $0°$ to $160°$. (b) The cross sections are displayed on a radial map.

underestimate of the IQMD + GEMINI model in the energy region around tens MeV. But the global uncertainty of the IQMD + GEMINI model is similar to the cases of the benchmark codes.

The predictions of the double differential cross sections of neutrons produced in $d + {}^{137}$Cs spallation at 500 MeV/nucleon are shown in Fig. 3. In panel (a), the cross sections are scaled with factors from 1 to 10^{-10}, for cases from $0°$ to $160°$. In panel (b), the cross sections are displayed on a radial map, in which the distance from the origin to curve refers to the value of cross section while the radial curve indicates the angles. It is shown that most high-energy neutrons are emitted forward. As an example, for 100 MeV, the cross section at $0°$ is 1.4 mb/MeV sr, while that at $160°$ is only 0.06 mb/MeV sr. The maximum of the neutron energy reaches to about 800 MeV, although its cross section is very low (about μb/MeV sr). In panel (a), there are obvious peaks around 500 MeV for the cases of $0°$ and $10°$. They are caused by the breakup of the incident deuterons. The neutron in the deuteron has a relatively large possibility of escaping because of the weak bounding of the deuteron. More interestingly, panel (b) shows that the most probable cross section for the escaped neutrons appears not at $0°$ but at $10°$.

In order to clarify the mechanism of the deuteron breakup in spallation reactions, the correlation of longitudinal momenta between neutron and proton from the deuteron after colliding with ^{137}Cs at 500 MeV/nucleon is shown in Fig. 4. The colors (or grayscale) in the figure refer to the non-normalized probabilities of the events for a given (p_{pz}, p_{nz}) correlation, where p_{pz} is the longitudinal momentum of the proton and p_{nz} is that of the neutron. One can distinguish four reaction channels from the obvious differences of the colors (or grayscale). They are explained in the following.

Elastic breakup. The yellow (or lightest gray level) pixels in the region $0.85 < p_{pz} < 1.0$ GeV/c and $0.85 < p_{pn} < 1.0$ GeV/c correspond to the elastic breakup of the deuteron in a peripheral collision, in which the deuteron breaks up into a proton and neutron almost without energy transferring to the target.

Neutron stripping. The green (or middle gray level) part on the right side ($0.85 < p_{pz} < 1.0$ GeV/c and $p_{pn} < 0.85$ GeV/c) represents the case of neutron stripping, in which the neutron in the deuteron is absorbed by the target, leaving the proton with momentum similar to the incident case.

Proton stripping. The green (or middle gray level) part on the top ($0.85 < p_{pn} < 1.0$ GeV/c and $p_{pz} < 0.85$ GeV/c) refers to proton stripping, in which the proton is absorbed by the target but the neutron is not.

Deuteron absorbing. For the remainder, the incident deuteron is absorbed. This means that the proton and neutron from the deuteron undergo multiple collisions, so that the distributions of the momenta are relatively uniform.

Figure 5 shows the contributions of deuteron absorbing, neutron stripping, proton stripping, and elastic breakup to the energy distribution of neutrons emitted at $10°$ in the $d + {}^{137}$Cs reaction at 500 MeV/nucleon. It is shown that the neutrons with energies from 100 to 420 MeV mainly
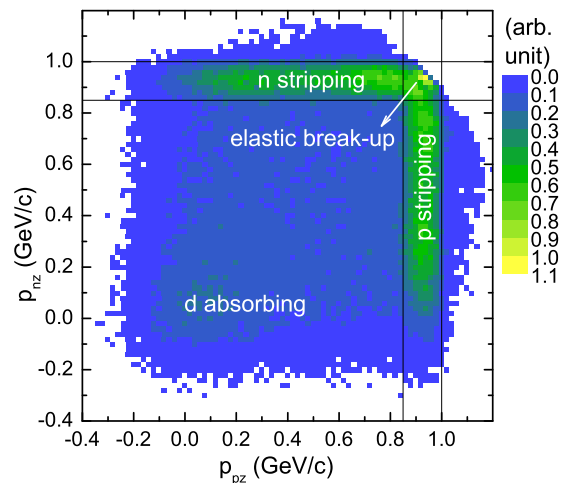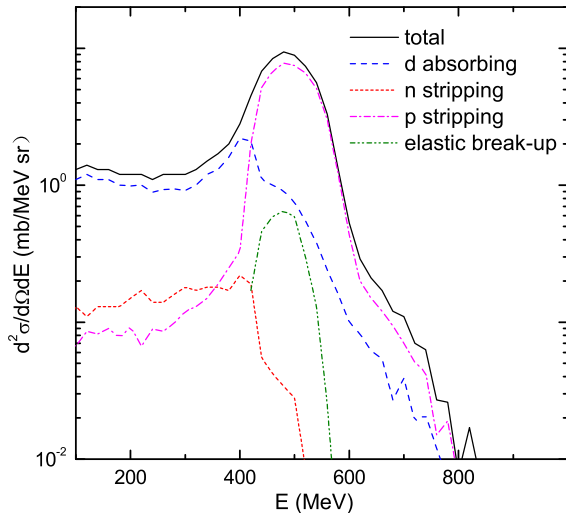

FIG. 4. Correlation of longitudinal momenta between neutron and proton from the deuteron after colliding with ^{137}Cs at 500 MeV/nucleon.

FIG. 5. Contributions of deuteron absorbing, neutron stripping, proton stripping, and elastic breakup to the energy distribution of neutrons emitted at $10°$ in $d + {}^{137}$Cs spallation at 500 MeV/nucleon.

FIG. 6. Plane of transverse momentum vs longitudinal momentum of (a) neutrons and (b) protons in ^{137}Cs $+ d$ spallation at 500 MeV/nucleon.

come from the deuteron absorbing channel, while those with energy larger than 420 MeV are mainly derived from the proton stripping channel. For the neutron stripping channel, the neutron experiences multiple collisions and then is emitted from the excited target nucleus. So the cross sections for the high energy part are very low. The elastic breakup channel also produces neutrons with energy around 500 MeV, but its cross sections are very low, only about 6% of the case for proton stripping.

The contributions of those four reaction channels to the energy distribution of protons are similar but the conditions between the proton and neutron are inverse. Those phenomena may be helpful in the research field of ADSs. First, if a subcritical reactor is driven by a deuteron beam (rather than a proton beam), one may enhance the portion of high-energy neutrons in the reactor [36]. Because the spallation cross sections for the LLFPs are larger than thermal cross sections, the LLFPs may be transmuted more effectively [37]. Second, deuteron-induced spallation may be applied as a high-energy neutron source, which is significant to measure the cross sections of neutron-induced spallation. Time-of-flight spectrometry may be applied to choose the neutron in the GeV region. The coincidence measurement of the high-energy proton in the elastic breakup channel is also possible. Last but not the least, the spallation in the neutron stripping channel is actually caused by the neutron. This may be applied to measure neutron-induced spallation. In the next subsection, we will study the last case in detail.

B. Inverse dynamics (^{137}Cs $+ d$)

Inverse dynamics, i.e., the interaction between the heavy-ion beam and the hydrogen or deuterium target, is usually applied to measure the isotopic production cross sections of residual nuclei in spallation. In this subsection, the inverse dynamics ^{137}Cs $+ d$ is considered. Figure 6 displays the plane of transverse momentum vs longitudinal momentum of neutrons
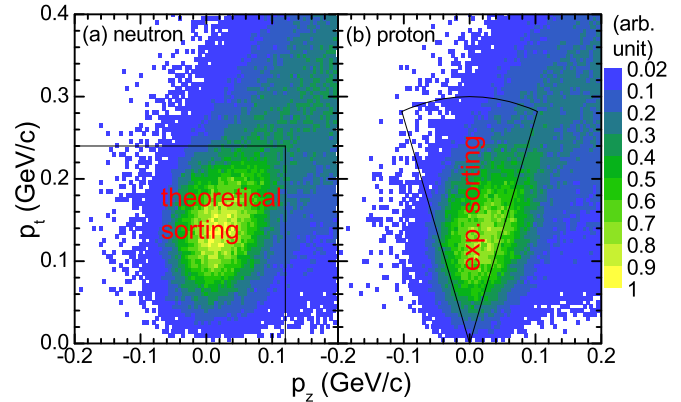
and protons in ^{137}Cs $+ d$ spallation at 500 MeV/nucleon. In fact, this kind of observable has been widely used in experiments, such as the plane of transverse momentum vs rapidity in Ref. [38]. The figure shows that the protons (or neutrons) can be emitted transversely with high probability in the low energy region. The most probable momentum in the longitudinal direction is zero, while that in the transverse direction is about 0.14 GeV/c. It should be noted that the zero longitudinal momentum of protons (or neutrons) in the inverse reaction ^{137}Cs $+ d$ corresponds to the incident momentum in the $d + {}^{137}$Cs reaction ($p_{pz} = 0.94$ GeV/c in Fig. 4). Or we conclude that the protons emitted transversely in the inverse reaction ^{137}Cs $+ d$ are derived from the neutron stripping and elastic breakup channels. That is to say the neutron stripping and elastic breakup channels are not only theoretical concepts but also can be sorted in experiments by detecting the low-energy protons in the transverse direction to the incident beam. On the other hand, the kinetic energy of the protons emitting transversely is about 10.4 MeV (2.0% of 500 MeV), while the bounding energy of the deuteron is 2.2 MeV (0.4% of 500 MeV). Based on the tiny energy absorbed by the proton compared to the incident energy per nucleon, it is suggested that, in the neutron stripping and elastic breakup channels, the ^{137}Cs nucleus interacts with the stripping neutron at nearly 500 MeV/nucleon. Or we say the neutron stripping and elastic breakup channels in the ^{137}Cs $+ d$ reaction may be equivalent to the ^{137}Cs $+ n$ spallation. An exact statement should be that the neutron stripping channel (without elastic breakup) in the ^{137}Cs $+ d$ reaction may be equivalent to the ^{137}Cs $+ n$ spallation. However, the recoil protons in Fig. 6 come from both neutron stripping and elastic breakup channels. One the other hand, the elastic breakup channel contributes little to the excitation of the ^{137}Cs. Thus the elastic breakup channel is taken into account in the equivalent method. In a similar way, the proton stripping and elastic breakup channels in the ^{137}Cs $+ d$ reaction may be equivalent to the ^{137}Cs $+ p$ spallation.

The proton stripping and the elastic breakup channels in ^{136}Xe $+ d$ collisions at 500 MeV/nucleon are sorted by finding a neutron with longitudinal momentum $p_z < 0.12$
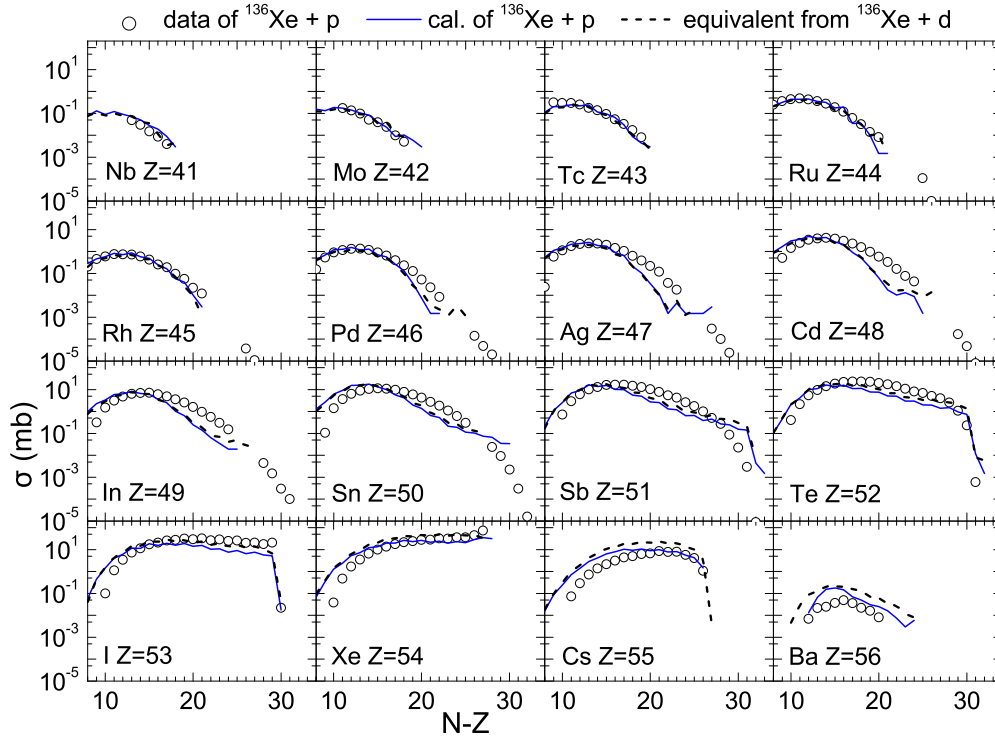
FIG. 7. Isotopic production cross sections of residual nuclei (Z from 41 to 56) produced in ^{136}Xe $+p$ at 500 MeV/nucleon. The experimental data, shown as open circles, are taken from Ref. [35]. The calculations by the IQMD + GEMINI model are shown as solid curves. The equivalents extracted from ^{136}Xe $+d$ at 500 MeV/nucleon are shown as dashed curves.

GeV/c and transverse momentum $p_t < 0.24$ GeV/c. This sorting method, as shown in Fig. 6(a), can only be realized theoretically. Experimentally, the the events can be sorted by placing the silicon detector in the vertical direction (e.g., to cover the angle from $70°$ to $110°$) and setting the maximum energy (such as 50 MeV). The experimental sorting is shown in Fig. 6(b).

In the model, the cross sections of the residual nuclei are calculated by

$$\sigma(Z, N) = \frac{N(Z, N)}{N_{event}} \pi b_{max}^2, \qquad (11)$$

where $N(Z, N)$ is number of the residual nuclei with charge number Z and neutron number N, N_{event} is number of the simulated events, b_{max} is the maximum impact parameter. Replacing the event number N_{event} by the sorting number of the events N_{sort}, one can calculate the equivalent cross sections of the residual nuclei,

$$\sigma_e(Z, N) = \frac{N(Z, N)}{N_{sort}} \pi b_{max}^2. \qquad (12)$$

Using the recoil neutrons sorted by $p_z < 0.12$ GeV/c and $p_t < 0.24$ GeV/c, as shown in Fig. 6(a), the equivalent cross sections in the proton-induced spallation are calculated from the ^{136}Xe $+d$ collision. In Fig. 7, the equivalent cross sections are compared to the cross sections in the ^{136}Xe $+p$ collision at 500 MeV/nucleon, including the data from Ref. [35] and the calculations by the IQMD + GEMINI model. Both the calculations and equivalents represent the data globally.

The discrepancies between the the calculations and the data mainly appear in the two sides of the peaks. Interestingly, the equivalent cross section from the ^{136}Xe $+d$ collision agrees with the calculations in the ^{136}Xe $+p$ collision, except for the residual nuclei that have a mass number near 136.

Using the recoil protons selected by both the theoretical sorting method [similar to that in Fig. 6(a)] and experimental sorting method [as shown in Fig. 6(b)], the equivalent cross sections in the neutron-induced spallation are calculated from the ^{136}Xe $+d$ collision. The equivalent cross sections are compared to the calculations of the ^{137}Cs $+n$ spallation at 500 MeV/nucleon, as shown in Fig. 8. One sees the considerable cross sections for $Z = 56$, which are caused by the inelastic NN collision. Once again, the equivalent cross sections agree with the calculations in the ^{136}Xe $+n$ collision. More importantly, the equivalent cross sections by both event sorting methods agree with each other. Note that the experimental sorting method does not select all recoil protons, as shown in Fig. 6(b). This provides convenience for equivalent measurement. Specifically, the trigger signal of the measurement can be provided by the the silicon detector, which is placed near the target and in the vertical direction of the beam. The solid angle depends on the area of the silicon detector and the distance between the target and the silicon detector. Since it is unnecessary to measure all the recoil protons, the silicon detector and its location are optional, as long as they detect some of the recoil protons.

In order to evaluate the equivalent method quantitatively, the ratios between the equivalent cross sections from the
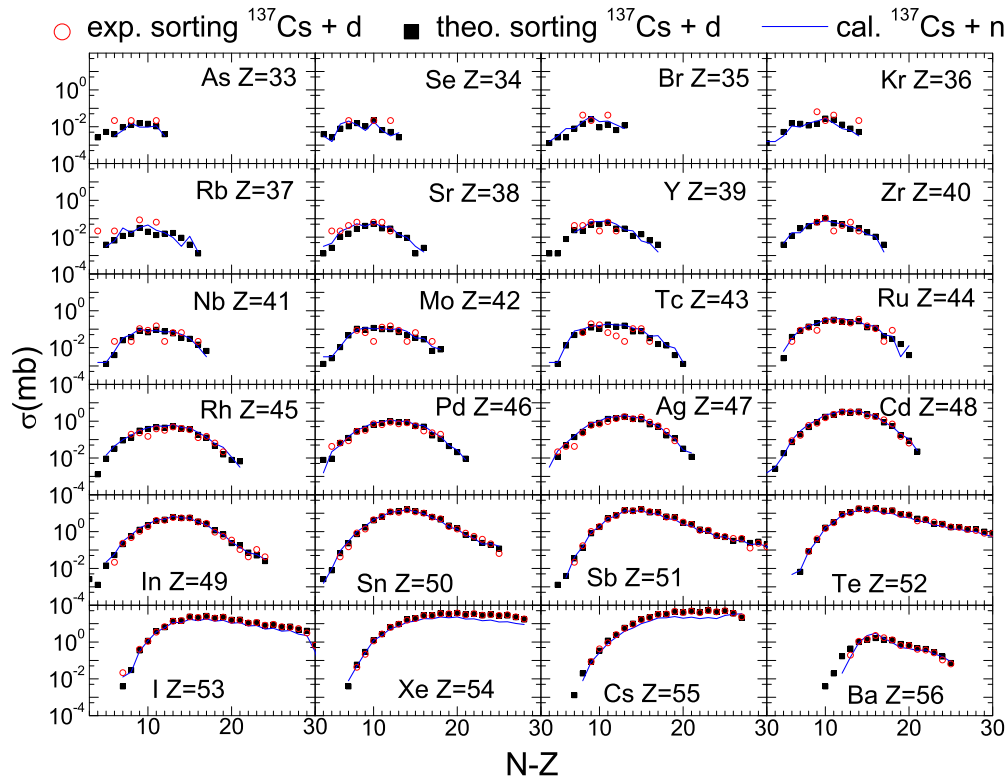
FIG. 8. Isotopic production cross sections of residual nuclei (Z from 33 to 56) produced in ^{137}Cs $+n$ spallation at 500 MeV/nucleon. The calculations by the IQMD + GEMINI model are shown as solid curves. The equivalents extracted from ^{137}Cs $+d$ at 500 MeV/nucleon are shown as solid squares.

^{136}Xe $+d$ collision and the calculations of the ^{136}Xe $+n$ collision are calculated. They are shown in Fig. 9 as functions of the differences between the neutron number and charge number and of the cross-section values. For most of these isotopes, the ratios are in the vicinity of 1. However, one also see the large ratios, almost 2.5 for some isotopes of Cs, and the small ratios reaching 0.4, such as that of ^{79}Br. In Fig. 9(b), it is found that the relations of the ratios and the cross sections are approximatively linear, in spite the isotopes of Xe and Cs and those with small cross sections. For the isotopes with cross

sections $\sigma < 0.02$ mb, the calculation error has a considerably great effect on them.

Figure 10 shows the distributions of the impact parameter and the excitation energy in the ^{137}Cs $+n$ collision and the equivalent events selected from the ^{137}Cs $+d$ collision. The distribution of the impact parameter the ^{137}Cs $+n$ collision is geometrical, which can be expressed as $d\sigma/db = 2\pi b$. The case of the equivalent events is in principle different from the geometrical one. For central collisions, both the proton and neutron from the deuteron will collide with the ^{137}Cs
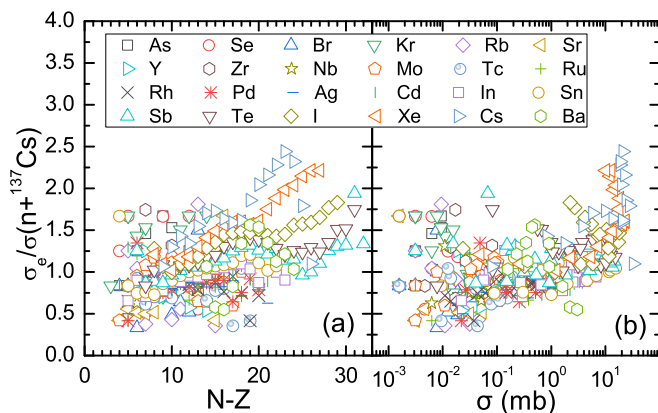

FIG. 9. Ratios between the equivalents and calculations in Fig. 8 as functions of (a) the differences between the neutron number and charge number and of (b) and the cross-section values.
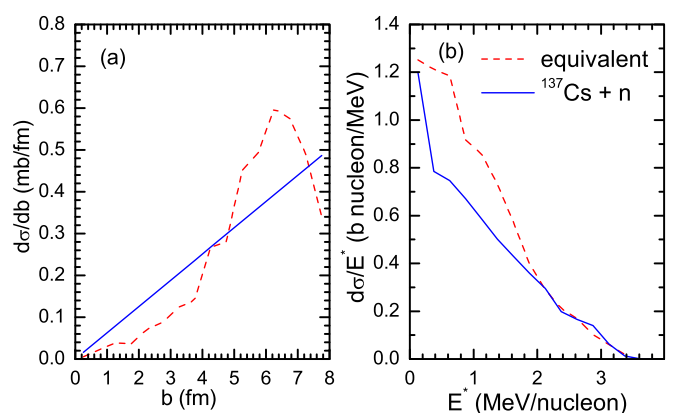

FIG. 10. Distributions of (a) the impact parameter and (b) the excitation energy in the ^{137}Cs $+n$ collision and the equivalent events selected from the ^{137}Cs $+d$ collision.

nucleus with large probability. The stripping is more likely to happen in a peripheral collision. Thus, compared to the geometrical case, one sees a larger cross section in the region of $5 < b < 7$ fm but a smaller one for $b < 4$ fm. From the distributions of the excitation energy shown in Fig. 10(b), one sees similar cross sections for high excitation energy. The differences appear for $E^* < 2$ MeV/nucleon and increase with decreasing excitation energy. Note that the events with smaller excitation energy contribute mainly to produce the residues with mass number near 137. This is why the errors of the equivalent method are large for Xe and Cs isotopes.

IV. CONCLUSION

In summary, by comparing the experimental data and the calculations of other models, the isospin-dependent quantum molecular dynamics (IQMD) model together with the code GEMINI are proved to be able to calculate the double differential cross sections of neutrons in spallation near 500 MeV. Then the deuteron breakup in $d + {}^{137}$Cs collisions at 500 MeV/nucleon is investigated. The $d + {}^{137}$Cs collision is divided into four channels, i.e., elastic breakup, neutron strip-

ping, proton stripping, and deuteron absorbing. It is suggested that the neutron stripping and elastic breakup channels, which may be sorted by detecting the recoil protons in the direction transverse to the incident beam, is equivalent to neutron-induced spallation. The sorting events from the ^{137}Cs $+ d$ collision are applied to calculate the equivalent cross sections of residue production and compared to those of the ^{137}Cs $+ n$ collision. It is found that the ratios between two cases are in the vicinity of 1 for most isotopes. But large differences appear for Xe and Cs isotopes. It is concluded that the deuteron-induced spallation may be promisingly applied to measure indirectly the cross sections in neutron-induced spallation. But before doing that, the equivalent method should be improved by studying further the dynamics of the neutron stripping in deuteron-induced spallation. On the other hand, the equivalent method needs further validation using experimental data.

[1] Y. Matsuo and H. Nei, An analysis of the historical trends in nuclear power plant construction costs: The Japanese experience, Energy Policy **124**, 180 (2019).

[2] J. Wallenius, Maximum efficiency nuclear waste transmutation, Ann. Nucl. Energy **125**, 74 (2019).

[3] D. Durant, Responsible action and nuclear waste disposal, Technol. Soc. **31**, 150 (2009).

[4] Z. Ma, R. P. Gamage, T. Rathnaweera, and L. Kong, Review of application of molecular dynamic simulations in geological high level radioactive waste disposal, Appl. Clay Sci. **168**, 436 (2019).

[5] S. Leray, F. Borne, S. Crespin, J. Fréhaut, X. Ledoux, E. Martinez, Y. Patin, E. Petibon, P. Pras, A. Boudard, R. Legrain, Y. Terrien, F. Brochard, D. Drake, J. C. Duchazeaubeneix, J. M. Durand, S. I. Meigo, G. Milleret, D. M. Whittal, W. Wlazlo, D. Durand, C. Le Brun, F. R. Lecolley, J. F. Lecolley, F. Lefebvres, M. Louvel, C. Varignon, F. Hanappe, S. Ménard, L. Stuttge, and J. Thun, Spallation neutron production by 0.8, 1.2, and 1.6 GeV protons on various targets, Phys. Rev. C **65**, 044621 (2002).

[6] B. Grambow and S. Bretesche, Geological disposal of nuclear waste: II. From laboratory data to the safety analysis—Addressing societal concerns, Appl. Geochem. **49**, 247 (2014).

[7] S. H. Hong and M. H. Kim, Neutronic investigation of waste transmutation option without partitioning and transmutation in a fusion-fission hybrid system, Nucl. Eng. Technol. **50**, 1060 (2018).

[8] Benefits, Potential, Impacts of Advanced Nuclear Fuel Cycles with Actinide Partitioning and Transmutation, Nuclear Science (2011).

[9] W. S. Yang, Y. Kim, R. N. Hill, T. A. Taiwo, and H. S. Khalil, Long-lived fission product transmutation studies, Nucl. Sci. Eng. **146**, 291 (2004).

[10] K. D. Dobbin, D. P. Jordheim, D. W. Wootan, and J. A. Rawlins, Transmutation of LWR high-level waste in LMRs, Trans. Am. Nucl. Soc. **64**, 122 (1991).

[11] T. Wakabayashi and N. Higana, Study on MA and FP transmutation in fast reactors, Prog. Nucl. Energy **32**, 555 (1998).

[12] W. S. Park, Y. H. Kim, C. K. Park, J. S. Chung, and C. H. Kim, A design study of ^{99}Tc and ^{129}I transmutation in the HYPER system, Nucl. Sci. Eng. **143**, 188 (2002).

[13] H. Nifeneckera, S. Davidb, J. M. Loiseauxa, and O. Meplan, Basics of accelerator driven subcritical reactors, Nucl. Instrum. Methods Phys. Res., Sect. A **463**, 428 (2001).

[14] H. Wang *et al.*, Spallation reaction study for the long-lived fission products in nuclear waste: Cross section measurements for ^{137}Cs, ^{90}Sr and ^{107}Pd using inverse kinematics method, Energy Procedia **131**, 127 (2017).

[15] B. Champine, M. E. Gooden, Krishichayan, E. B. Norman, N. D. Scielzo, M. A. Stoyer, K. J. Thomas, A. P. Tonchev, W. Tornow, and B. S. Wang, Measurement of the ^{169}Tm$(n, 3n)^{167}$Tm cross section and the associated branching ratios in the decay of ^{167}Tm, Phys. Rev. C **93**, 014611 (2016).

[16] S. Henderson, Report from the DOE ADS White Paper Working Group, in Thorium Energy Conference (2011).

[17] R. Plukien, A. Plukis, L. Juodis, V. Remeikis, O. Šalkauskas, D. Ridikas, and W. Gudowski, Transmutation considerations of LWR and RBMK spent nuclear fuel by the fusion-fission hybrid system, Nucl. Eng. Des. **330**, 241 (2018).

[18] T. Mukhopadhyay, J. Lahiri, and D. N. Basu, Erratum: Cross sections of neutron-induced reactions [Phys. Rev. C **82**, 044613 (2010)], Phys. Rev. C **83**, 039902(E) (2011).

[19] V. P. Eismont, A. V. Prokofyev, A. N. Smirnov, K. Elmgren, J. Blomgren, H. Condé, J. Nilsson, N. Olsson, T. Rönnqvist, and E. Tranéus, Relative and absolute neutron-induced fission cross sections of ^{208}Pb, ^{209}Bi, and ^{238}U in the intermediate energy region, Phys. Rev. C **53**, 2911 (1996).

[20] V. I. Gol'danskii, E. Z. Tarumov, and V. S. Pen'kina, Fission of heavy nuclei by high-energy neutrons, Dokl. Akad. Nauk SSSR Inst. Chem. Phys. **101**, 1027 (1955).

[21] P. W. Lisowski, C. D. Bowman, G. J. Russell, and S. A. Wender, The los alamos national laboratory spallation neutron sources, Nucl. Sci. Eng. **106**, 208 (1990).

[22] J. C. David, Spallation reactions: A successful interplay between modeling and applications, Eur. Phys. J. A **51**, 68 (2015).

[23] J. Su, L. Zhu, and C. Guo, Influence of the nuclear level density on the odd-even staggering in ^{56}Fe $+ p$ spallation at energies from 300 to 1500 MeV/nucleon, Phys. Rev. C **97**, 054604 (2018).

[24] J. Xu, L. W. Chen, ManYee Betty Tsang, H. Wolter, Y. X. Zhang, J. Aichelin, M. Colonna, D. Cozma, P. Danielewicz, Z. Q. Feng, A. LeFevre, T. Gaitanos, C. Hartnack, K. Kim, Y. Kim, C. M. Ko, B. A. Li, Q. F. Li, Z. X. Li, P. Napolitani, A. Ono, M. Papa, T. Song, J. Su, J. L. Tian, N. Wang, Y. J. Wang, J. Weil, W. J. Xie, F. S. Zhang, and G. Q. Zhang, Understanding transport simulations of heavy-ion collisions at 100*A* and 400*A* MeV: Comparison of heavy-ion transport codes under controlled conditions, Phys. Rev. C **93**, 044609 (2016).

[25] Y. X. Zhang, Y. J. Wang, M. Colonna, P. Danielewicz, A. Ono, M. B. Tsang, H. Wolter, J. Xu, L. W. Chen, D. Cozma, Z. Q. Feng, S. Das Gupta, N. Ikeno, C. M. Ko, B. A. Li, Q. F. Li, Z. X. Li, S. Mallik, Y. Nara, T. Ogawa, A. Ohnishi, D. Oliinychenko, M. Papa, H. Petersen, J. Su, T. Song, J. Weil, N. Wang, F. S. Zhang, and Z. Zhang, Comparison of heavy-ion transport simulations: Collision integral in a box, Phys. Rev. C **97**, 034625 (2018).

[26] J. Aichelin, "Quantum" molecular dynamics—a dynamical microscopic n-body approach to investigate fragment formation and the nuclear equation of state in heavy ion collisions, Phys. Rep. **202**, 233 (1991).

[27] C. Hartnack, L. Zhuxia, L. Neise, G. Peilert, A. Rosenhauer, H. Sorge, J. Aichelin, H. Stöcker, and W. Greiner, Quantum molecular dynamics a microscopic model from UNILAC to CERN energies, Nucl. Phys. A **495**, 303 (1989).

[28] J. Cugnon, D. L'Hôte, and J. Vandermeulen, Simple parametrization of cross-sections for nuclear transport studies up to the GeV range, Nucl. Instrum. Methods Phys. Res. B **111**, 215 (1996).

[29] D. D. S. Coupland, W. G. Lynch, M. B. Tsang, P. Danielewicz, and Y. X. Zhang, Influence of transport vari- ables on isospin transport ratios, Phys. Rev. C **84**, 054603 (2011).

[30] A. Ono *et al.*, Comparison of heavy-ion transport simulations: Collision integral with pions and Δ resonances in a box, Phys. Rev. C **100**, 044617 (2019).

[31] R. J. Charity, M. A. McMahan, G. J. Wozniak, R. J. McDonald, L. G. Moretto, D. G. Sarantites, L. G. Sobotka, G. Guarino, A. Pantaleo, L. Fiore, A. Gobbi, and K. D. Hildenbrand, Systematics of complex fragment emission in niobium-induced reactions, Nucl. Phys. A **483**, 371 (1988).

[32] H. Gruppelaar and G. Reffo, Some properties of the width fluctuation factor, Nucl. Sci. Eng. **62**, 756 (1977).

[33] K. Ishibashi, H. Takada, T. Nakamoto, N. Shigyo, K. Maehata, N. Matsufuji, S. Meigo, S. Chiba, M. Numajiri, Y. Watanabe, and T. Nakamura, Measurement of neutron-production double-differential cross sections for nuclear spallation reaction induced by 0.8, 1.5 and 3.0 GeV protons, J. Nucl. Sci. Technol. **34**, 529 (1997).

[34] https://www-nds.iaea.org/spallations

[35] L. Giot, J. A. Alcántara-Núñez, J. Benlliure, D. Pérez-Loureiro, L. Audouin, A. Boudard, E. Casarejos, T. Enqvist, J. E. Ducret, B. Fernández-Domínguez, M. Fernández Ordóñez, F. Farget, A. Heinz, V. Henzl, D. Henzlova, A. Kelić-Heil, A. Lafriaskh, S. Leray, P. Napolitani, C. Paradela, J. Pereira, M. V. Ricciardi, C. Stéphan, K. H. Schmidt, C. Schmitt, L. Tassan-Got, C. Villagrasa, C. Volant, and O. Yordanov, Isotopic production cross sections of the residual nuclei in spallation reactions induced by ^{136}Xe projectiles on proton at 500 AMeV, Nucl. Phys. A **899**, 116 (2013).

[36] S. R. Hashemi-Nezhad, W. Westmeier, M. Zamani-Valasiadou, B. Thomauske, and R. Brandt, Optimal ion beam, target type and size for accelerator driven systems: Implications to the associated accelerator power, Ann. Nucl. Energy **38**, 1144 (2011).

[37] K. Tsujimoto, T. Sasa, K. Nishihara, T. Takizuka, and H. Takano, Accelerator-driven system for transmutation of high-level waste, Prog. Nucl. Energy **37**, 339 (2000).

[38] B. Hong and Y. J. Kim, Review of application of molecular dynamic simulations in geological high level radioactive waste disposal, Phys. Rev. C **66**, 034901 (2002).